A Fast Continuous Max-Flow Approach to Potts Model

Jing Yuan[1], Egil Bae[2], Xue-Cheng Tai[2], and Yuri Boykov[1]

[1] Computer Science Department, University of Western Ontario
London, Ontario, Canada N6A 5B7
cn.yuanjing@gmail.com, yuri@csd.uwo.ca
[2] Department of Mathematics, University of Bergen, Bergen, Norway
Egil.Bae@math.uib.no, tai@mi.uib.no

Abstract. In this work, we study a convex relaxation approach to partition the spatially continuous image domain into multiple regions with minimal total perimeter. Its corresponding model over a discrete image graph, the so-called Potts model, can be addressed approximately by graph-cut based α-expansion, which often generate visible metrication artifacts, hence impact the accuracy of image segmentation. Existing convex relaxation formulations of the Potts model, in the spatially continuous setting, use the total-variation based energy functionals which directly encode the isotropic perimeter costs and prefer tight partitioning without such metrication errors. These formulations are analogous to the multi-way 'min-cut' problems over graphs. In this paper, we propose a novel continuous convex optimization model in the form of flow maximization, so-called the continuous max-flow model, and demonstrate its duality to a standard convex relaxation formulation of the Potts model. The proposed continuous max-flow model leads to a new variational perspective of the studied image partitioning problem. In addition, its flow-maximization formulation directly leads to a new and fast max-flow based algorithm which has great numerical advantages: avoids extra computational load to enforce the pixelwise simplex constraint, which is the essential step in previous approaches, and naturally allows parallel computing over different labels. Practical experiments show its significant outperformance over the previous state of the art convex optimization approaches to the continuous Potts model, in terms of efficiency and quality.

1 Introduction

To label an image domain pixelwise with the given n discrete labels $l_1, \ldots l_n$, subject to some optimization criterion, gives rise to an effective tool to model many practical problems in image processing and computer vision [34] through Markov Random Fields (MRF). Potts model [37] corresponds to one special case of such Markov Random Field (MRF) over the image graph [29], which computes the graph partition with the minimal total perimeter of the one-label (constant) regions. It does not favor any particular order of the labels, in comparison to another similar model introduced by Ishikawa [21] which partitions the image graph with multiple linearly ordered labels (overlapped to each other). The MRF-based energy function proposed by Potts model is the sum of the unary potential defined on each graph node and the pairwise potential given on each graph edge. It is typically NP hard; only the approximate algorithms are

available: for example, via α-expansion or α-β swap [5] and some LP relaxations [25, 38]. For the special case with 2 labels, the resulting 0-1 optimization problem can be solved exactly and globally by graph cuts [17], provided that all the pairwise potentials are sub-modular [24]. A significant disadvantage of the graph-based approach to Potts model is that the computation results are often biased by the discrete image grid, which introduces visible metrication errors. Such visual artefacts can be largely reduced by either adding more neighboring nodes [4, 23] or applying high-order cliques [22]. However, both of them amounts to a great increase of computation complexities and memory load.

Parallel to the developments of graph-based approaches, variational methods have been proposed to tackle the same Potts model over a spatially continuous configuration, which properly avoid the metrication errors along with the discrete image graph. In this regard, the level-set method introduces the most direct and natural way to encode the piecewise constant labeling functions used in Potts model. Its related computation provides an efficient way to resolve the partitions with a sub-grid accuracy, see e.g. [33, 10, 7] and also the piecewise constant level-set method (PCLSM) [31, 30]. Unfortunately, the level-set method is essentially formulated in a non-convex manner, for which computation often gets stuck in a local minima and its result highly depends on the given initial conditions.

In contrast, the convex relaxation approaches, e.g. [32, 44, 36, 8, 2, 27], initially formulate Potts model by solving a convex optimization problem, where assigning an unique label to each pixel is encoded by the pixel-wise simplex constraint and the minimization of the total perimeter is formulated by the sum of total-variation functions. In comparison to the level-set method, such convex optimization based methods achieve great advantages in numerics such that fast and reliable algorithms can be easily obtained through standard convex optimization theories [3]. Since the strict mathematical proof of the exactness of the convex relaxation approach to the nonconvex Potts model is still open and argued [8], its computation result can only be accepted as suboptimal. One can still claim the convex relaxation method gives a solution which is close to the exact global minimum [28]. Practical experiments confirmed this.

In this paper, we study the convex relaxation approach to the Potts problem formulated in the spatially continuous settings, which is also called *convex relaxed Potts model*. In [44, 27], such convex optimization problem is solved directly through the minimization over the n labeling functions, for which extra computation cost is introduced to explore the pointwise simplex constraint at each iteration. In this regard, Bae et al [2] proposed an equivalent dual model and its associated smoothing formulation based on the maximum entropy regularization, which effectively avoids the extra step to handle simplex constraint at each pixel and leads to a much simpler numerical scheme. In this work, we investigate the *convex relaxed Potts model* in the manner of primal-dual and propose the novel continuous max-flow model. It carries a new flow-maximization theory which is dual to the *convex relaxed Potts model*. To the best of our knowledge, none of previous works introduces such a max-flow theory to the Potts problem. On the other hand, the minimum cut of a graph is often studied and computed over its dual maximal flow formulation; most efficient algorithms of graph-cuts were designed and explained in such a flow maximization manner [11]. For Potts model which results

in computing the 'multi-way cut', the graph-based optimization methods, such as α-expansion, also work by performing the max-flow algorithm iteratively. With respect to this, we show the proposed continuous max-flow scheme to the *convex relaxed Potts model* is also different from the standard max-flow approaches. This work extends our previous conference proceeding paper [42].

1.1 Contributions

We summarize our main contributions as follows:

- We propose a novel continuous max-flow formulation to the convex relaxed Potts model over a continuous image domain. We show that the proposed continuous max-flow model and the convex relaxed Potts model are equivalent or dual to each other, hence the convex relaxed Potts problem can be computed through tackling the corresponding max-flow problem.
- Mathematical analysis on the continuous max-flow model leads to a new interpretation of partitioning the given image domain into multiple regions under the variational perspective. By this, the essential connections between 'flow saturation' and 'cut' are revealed.
- The proposed continuous max-flow model directly results in a new multiplier-based max-flow algorithm based on the standard convex optimization theory. The numerical advantages of the continuous max-flow based algorithm over previous works are generalized as follows: first, it avoids the extra projections onto the pixelwise simplex constraint within each outer iteration as in [44, 27]; compared to [2, 26], it exactly solves (8) without any smoothing procedure; in addition, it is globally optimized based on an efficient and reliable multiplier-based max-flow algorithm, in contrast to the projected-gradient method [8, 35] whose convergence may suffer from uncareful step-sizes and result in a sub-optima.
- Experiments show a faster convergence rate, about 4 times, than [44, 27]. In addition, the proposed max-flow based algorithm has a parallelism-friendly framework over labeling functions which can be easily implemented and accelerated on modern computing platforms, e.g. GPU.

2 Previous Works: Convex Relaxation Approaches

In this section, we first introduce the *convex relaxed Potts model* and review previous convex relaxation approaches. To motivate the continuous max-flow model to the *convex relaxed Potts model*, we also revisit the recent studies on the duality of the continuous max-flow and min-cut formulations, proposed in [40, 1].

2.1 Convex Relaxed Potts Model

The Potts model originates from the statistical physics [37] and its spatially continuous version can be stated by partitioning the continuous image domain Ω into n disjoint

subdomains $\{\Omega_i\}_{i=1}^n$ based on the following optimization criterion:

$$\min_{\{\Omega_i\}_{i=1}^n} \quad \sum_{i=1}^n \int_{\Omega_i} \rho(l_i, x)\, dx + \alpha \sum_{i=1}^n |\partial\Omega_i| \tag{1}$$

$$\text{s.t.} \quad \cup_{i=1}^n \Omega_i \,=\, \Omega\,; \quad \Omega_k \cap \Omega_l \,=\, \emptyset\,, \quad \forall k \neq l \tag{2}$$

where $|\partial\Omega_i|$ measures the perimeter of each disjoint subdomain Ω_i, $i = 1 \ldots n$; the function $\rho(l_i, x), i = 1 \ldots n$, evaluates the cost of assigning the label l_i to the specified position $x \in \Omega$ and the positive $\alpha > 0$ gives the trade-off between the two terms. Obviously, Potts model (1) favors the labeling with 'tight' boundaries. As a special case, the piecewise constant Mumford-Shah functional can be encoded, in terms of (1), by $\rho(l_i, x) = |I(x) - l_i|^p$ where $l_1 \ldots l_n$ are the given grayvalue constants.

Let $u_i(x), i = 1 \ldots n$, denote the indicator function of the disjoint subdomain Ω_i, i.e.

$$u_i(x) \,:=\, \begin{cases} 1\,, & x \in \Omega_i \\ 0\,, & x \notin \Omega_i \end{cases}\,, \quad i = 1 \ldots n\,. \tag{3}$$

The perimeter of each disjoint subdomain Ω_i can be evaluated by

$$|\partial\Omega_i| \,=\, \int_\Omega |\nabla u_i|\; dx\,, \quad i = 1 \ldots n\,. \tag{4}$$

In view of (3) and (4), the Potts model (1) can then be rewritten as

$$\min_{u_i(x)\in\{0,1\}} \sum_{i=1}^n \int_\Omega \left\{ u_i(x)\rho(l_i, x) \,+\, \alpha\, |\nabla u_i| \,\right\} dx\,, \;\; \text{s.t.} \;\; \sum_{i=1}^n u_i(x) \,=\, 1\,,\; \forall x \in \Omega \tag{5}$$

where the constraints on $u_i(x)$, $i = 1 \ldots n$, in (5) just corresponds to the condition (2), i.e. each image pixel can be assigned to one and only on region.

Clearly, the Potts model (5) is nonconvex due to the binary configuration of each function $u_i(x) \in \{0, 1\}$. The *convex relaxed Potts model* was proposed, where such binary constraints were relaxed to the convex interval $[0, 1]$ and approximates (5) by the reduced convex optimization problem [8, 27, 2]:

$$\min_{u\in S} \sum_{i=1}^n \int_\Omega u_i(x)\, \rho(l_i, x)\, dx \,+\, \alpha \sum_{i=1}^n \int_\Omega |\nabla u_i|\; dx \tag{6}$$

where S is the convex constrained set of $u(x) := (u_1(x), \ldots, u_n(x))$:

$$S \,=\, \{u(x)\,|\,(u_1(x), \ldots, u_n(x)) \,\in\, \triangle_+\,,\; \forall x \in \Omega\,\}\,, \tag{7}$$

$\triangle_+$ is the simplex set, i.e.

$$\text{for } \forall x \in \Omega\,, \quad \sum_{i=1}^n u_i(x) \,=\, 1\,; \quad u_i(x) \in [0, 1]\,, \quad i = 1 \ldots n\,.$$

The computation result of the convex relaxed Potts model (6) gives an approximate solution to the multi-terminal 'cut' problem (5), i.e. the Potts model.

Previous Works In [44], Zach et al introduced an alternating optimization approach to solve (6) in a numerically splitting way:

$$\min_{u,v\in S} \sum_{i=1}^{n} \int_{\Omega} v_i(x)\, \rho(l_i, x)\, dx \; + \frac{1}{2\theta} \|u - v\|^2 \; + \; \alpha \sum_{i=1}^{n} \int_{\Omega} |\nabla u_i| \; dx \,.$$

Within each iteration, two sequential sub-steps are taken to tackle the total-variation term and explore the pointwise simplex constraint S respectively. Obviously, when θ takes a value small enough, the above convex optimization problem well approximates the convex relaxed Potts model (6).

In [27], a Douglas-Rachford splitting algorithm was proposed to solve a quite similar problem as (6), for which a variant of the total-variation term is considered:

$$\int_{\Omega} \sqrt{|\nabla u_1(x)|^2 + \ldots + |\nabla u_n(x)|^2}\, dx \,.$$

As in [44], the proposed splitting procedure involves an outer loop with two sequential steps: the first step solves a total-variation minimization problem iteratively until convergence, while the second step projects the current solution to the pixel-wise simplex constraint set S. In [26] Nestorov's algorithm was applied, however this algorithm does not solve the problem exactly, only within a suboptimality bound.

In [8, 35], the authors introduced another convex relaxation based on a multi-layered configuration, which was shown to be tighter. More complex constraints on the dual variable p were given to avoid multiple countings. The number of constraints grow quadratically in n instead of linearly, which complicates computation. In addition, an iterative primal-dual projected-gradient scheme was applied to achieve the minimum.

In contrast to [44, 27, 8, 35], Bae at al [2] proposed not to directly tackle the labeling function of the convex relaxed Potts problem (6), but solve its equivalent dual formulation:

$$\sup_{p_i \in C_\alpha} \int_{\Omega} \left\{ \min \left(\rho(l_1, x) + \operatorname{div} p_1 \;\; \ldots \;\; \rho(l_n, x) + \operatorname{div} p_n \right) \right\} dx \,. \tag{8}$$

where the functions $\operatorname{div} p_i$, $i = 1 \ldots n$, correspond to the total-variation terms under the primal-dual perspective and the convex set C_α is defined as

$$C_\alpha \; = \; \{ p \,|\, \|p\|_\infty \leq \alpha \,,\; p_n|_{\partial\Omega} = 0 \} \,. \tag{9}$$

Once the optimal functions $p_i^*(x)$, $i = 1 \ldots n$, are resolved, the labeling functions $u_i(x)$, $i = 1 \ldots n$, can be simply recovered by

$$u_k^*(x) \; = \; \begin{cases} 1 \;\; \text{if } k = \arg\min_{i=1\ldots n} \;\; \rho(l_i, x) + \operatorname{div} p_i^*(x) \\ 0 \;\; \text{otherwise} \end{cases} \,. \tag{10}$$

provided the above argmin is unique.It was further shown by [2] that the non-smooth dual function of (8) can be well approximated by the maximization of a smooth energy function, i.e.

$$\sup_{p_i \in C_\lambda} \; -s \int_{\Omega} \left\{ \log \sum_{i=1}^{n} \exp\left(\frac{-f_i - \operatorname{div} p_i}{s}\right) \right\} dx \,, \tag{11}$$

where $s > 0$ is the smoothness parameter. Such a smooth dual model (11) approaches (8) with an additional maximum-entropy regularization and can be solved efficiently by the simple and reliable algorithmic scheme due to its smoothness and convexity.

2.2 Continuous Max-Flow and Min-Cut Model

Now we introduce the recent study of the continuous max-flow model, proposed by Yuan et al [40, 39], to image segmentation, i.e. the continuous min-cut problem. Yuan et al proved that the proposed continuous max-flow model is dual to the continuous min-cut problem studied in [32, 6]. Such duality is directly analogous to the classical theory of max-flow and min-cut [14]:

Given the continuous image domain Ω and two terminals: the source s and the sink t (see the figure (a) of Fig. 1), link s and t to each image pixel $x \in \Omega$. We assume that for each $x \in \Omega$, there are three types of flows: the source flow $p_s(x) \in \mathbb{R}$ directed from the source s to x, the sink flow $p_t(x) \in \mathbb{R}$ directed from x to the sink t and the spatial flow field $p(x) \in \mathbb{R}^2$ around x. The three flow fields are constrained by the capacities:

$$p_s(x) \,\leq\, C_s(x)\,, \quad p_t(x) \,\leq\, C_t(x)\,, \quad |p(x)| \,\leq\, C(x)\,; \quad \forall x \in \Omega\,. \tag{12}$$

In addition, for $\forall x \in \Omega$, all flows are balanced, i.e. the flow conservation condition

$$(p_t - p_s + \operatorname{div} p)(x) \,=\, 0\,, \quad \text{a.e. } x \in \Omega\,. \tag{13}$$

Then, the continuous max-flow formulation is given by maximizing the total flow from the source s:

$$\sup_{p_s, p_t, p} \int_\Omega p_s \, dx \tag{14}$$

subject to flow constraints (12) and (13).

Yuan et al [40, 39] proved that such continuous max-flow model (14) is equivalent to the continuous min-cut problem proposed in [32, 6]:

$$\min_{u(x)\in[0,1]} \int_\Omega (1-u) C_s \, dx + \int_\Omega u C_t \, dx + \int_\Omega C(x)\, |\nabla u| \, dx\,. \tag{15}$$

Actually, the two convex models (15) and (14) are dual to each other: in the continuous max-flow model (14), the labeling function $u(x)$ works as the multiplier to the flow conservation condition (13). Moreover, an efficient and reliable multiplier-based max-flow algorithm can be built up through (14).

Based on the works [40, 39], Bae et al [1] further developed a continuous max-flow approach to the continuous cut problem for multiple linearly ordered labels. Its theory corresponds to the study of multi-layered graph-cut developed by Ishikawa [21].

3 Continuous Max-Flow Model

Motivated by the works [40, 39, 1], we propose and study a new continuous max-flow approach to the convex relaxed Potts model (6). In this section, we first introduce the novel continuous max-flow model and its associated flow configurations in the spatially continuous setting. We show its equivalence to the investigated convex relaxed Potts model (6) under a new variational perspective.

3.1 Flow-Maximization Configuration and Model

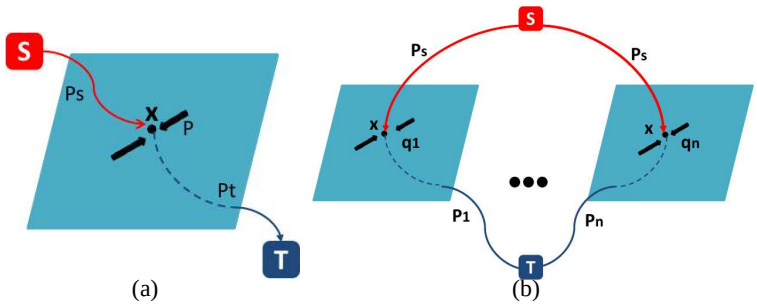

Fig. 1. (a) Continuous settings of max-flow with two labels; (b) Continuous configuration of max-flow with n labels.

Spatially Continuous Configurations Now we define the spatially continuous configuration of the max-flow model with n labels, see figure (b) of Fig. 1:

1. n copies Ω_i, $i = 1 \dots n$, of the image domain Ω are given in parallel;
2. For each position $x \in \Omega$, the source flow $p_s(x)$ tries to stream from the source s to x at each copy Ω_i, $i = 1 \dots n$, of Ω. The source flow field $p_s(x)$ is the same for each Ω_i, $i = 1 \dots n$, i.e. $p_s(x)$ is unique for all Ω_i, $i = 1 \dots n$;
3. For each position $x \in \Omega$, the sink flow $p_i(x)$, $i = 1 \dots n$, is directed from x at Ω_i to the sink t. In contrast to the source flow field $p_s(x)$, the n sink flow fields $p_i(x)$, $i = 1 \dots n$, mostly are different from each other;
4. The spatial flow fields $q_i(x)$, $i = 1 \dots n$, are defined within each copy Ω_i, $i = 1 \dots n$. They may also be different from each other.

Continuous Max-Flow Model Based on such spatially contiuous settings, we give the capacity and conservation constraints on flows, which are similar as (12) and (13): for flows $p_i(x)$ and $q_i(x)$ at each $x \in \Omega$, as follows:

$$|q_i(x)| \leq C_i(x)\,, \quad p_i(x) \leq \rho(l_i, x)\,, \quad i = 1 \dots n\,, \ \ \forall x \in \Omega; \tag{16}$$

$$\big(\operatorname{div} q_i - p_s + p_i\big)(x) = 0\,, \quad i = 1 \dots n\,, \ \ \text{a.e. } x \in \Omega. \tag{17}$$

Note: there is no constraint on the source flow function $p_s(x)$.

Therefore, we propose the respective continuous max-flow model, over all the flow functions $p_s(x)$, $p(x) := (p_1(x), \dots, p_n(x))$ and $q(x) := (q_1(x), \dots, q_n(x))$, as follows:

$$\sup_{p_s, p, q} \big\{ P(p_s, p, q) := \int_\Omega p_s \, dx \big\} \tag{18}$$

subject to the flow constraints (16) and (17).

In the following section, we introduce the equivalent models of the continuous max-flow formulation (18). We show its equivalent dual model is just the convex relaxed Potts model (6) provided $C(x) = \alpha$ is constant.

Preliminary Remarks and Connections The continuous max-flow model (18) tries to perform the maximization of the total source flow $p_s(x)$ over the whole image domain Ω subject to certain flow capacity and conservation conditions. It is easy to notice that at the same place x of each Ω_i, $i = 1 \dots n$, in view of the flow conservation condition (17), we have

$$p_s(x) \;=\; \operatorname{div} q_i(x) + p_i(x)\,, \quad i = 1 \dots n\,. \tag{19}$$

Observe the righthand of (19) and the flow capacity constraints given in (16), $p_s(x)$ is thus constrained and should be consistent to all the n flow configurations of $\operatorname{div} q_i(x) + p_i(x)$, $i = 1 \dots n$, at x. It naturally boils down to

$$p_s(x) \;=\; \min\big(\operatorname{div} q_1(x) + p_1(x), \dots, \operatorname{div} q_n(x) + p_n(x)\big)\,, \quad \forall x \in \Omega\,. \tag{20}$$

In this regard, we can prove

Proposition 1. *The proposed continuous max-flow model* (18) *is equivalent to*

$$\sup_{|q_i(x)| \le C_i(x)} \int_\Omega \big\{ \min\big(\rho(l_1, x) + \operatorname{div} q_1(x), \dots, \rho(l_n, x) + \operatorname{div} q_n(x)\big)\big\}\, dx\,. \tag{21}$$

Proof. Following the result (20), the continuous max-flow model (18) can be equally reformulated by

$$\sup_{p(x), q(x)} \int_\Omega \big\{ \min\big(p_1(x) + \operatorname{div} q_1(x), \dots, p_n(x) + \operatorname{div} q_n(x)\big)\big\}\, dx$$

subject to the flow capacity constraints (16).

Given $\lambda(x) := (\lambda_1(x), \dots, \lambda_n(x)) \in S$ where S denotes the piecewise simplex constraint (7), the above formulation can then be rewritten as

$$\sup_{p(x), q(x)} \min_{\lambda(x)} \int_\Omega \Big\{ \sum_{i=1}^n \lambda_i(x) \big(p_i(x) + \operatorname{div} q_i(x)\big)\Big\}\, dx\,. \tag{22}$$

Then it is easy to see that the maximization over $p_i(x) \le \rho(l_i, x)$, $i = 1 \dots n$, is consistent to the constraint $\lambda(x) \in S$. By simple variation computations over $p(x)$ and $\lambda(x)$, (22) just amounts to (21).

The result (21) of Prop. (1) simply discovers the nonsmooth dual model (8) proposed by [2], when $C_i(x) = \alpha$ are constant.

In addition, observing the conclusion (20), we can regard each image copy Ω_i, $i = 1 \dots n$, together with the constrained sink flow field $p_i(x)$ and the spatial flow field $q_i(x)$ given in (16), as a 'filter' F_i whose filtering capacity at $x \in \Omega$ is constrained by $\operatorname{div} q_i(x) + p_i(x)$ along with (16), i.e. the passing source flow $p_s(x)$ at each x does

not overflow the minimal flow allowed by the n 'filter' configurations. Then one can explain the continuous max-flow model (18) such that all the filters F_i, $i = 1, \ldots, n$, are layered one by one and the source flow $p_s(x)$ tries to pass such a stack of such 'filters' in one time. It is obvious that $p_s(x)$ is bottlenecked by the minimum capacity of $\operatorname{div} q_i(x) + p_i(x)$, $i = 1 \ldots n$. In such a 'filter' configuration, (18) aims to maximize the total flow passing through this 'filter' set.

3.2 Equivalent Primal-Dual Formulation

By the introdution of the multiplier functions $u_i(x)$, $i = 1 \ldots n$, to the n flow conservation equalities (17), then we have the equivalent primal-dual model of (18) as follows:

$$\sup_{p_s,p,q} \inf_{u} \Big\{ E(p_s, p, q; u) \;:=\; \int_\Omega p_s \, dx \;+\; \sum_{i=1}^{n} \int_\Omega u_i (\operatorname{div} q_i - p_s + p_i) \, dx \Big\} \qquad (23)$$
$$\text{s.t.} \quad p_i(x) \;\le\; \rho(\ell_i, x)\,, \quad |q_i(x)| \;\le\; C_i(x)\,; \quad i = 1 \ldots n$$

where $u(x) := (u_1(x), \ldots, u_n(x))$.

Rearranging the energy function $E(p_s, p, q; u)$ of (23), we have

$$E(p_s, p, q; u) \;=\; \int_\Omega \big\{ (1 - \sum_{i=1}^{n} u_i)\, p_s \;+\; \sum_{i=1}^{n} u_i \, p_i \;+\; \sum_{i=1}^{n} u_i \, \operatorname{div} q_i \big\} \, dx \qquad (24)$$

For the primal-dual model (23), the conditions of the minimax theorem (see e.g., [12] Chapter 6, Proposition 2.4) are all satisfied. That is, the constraints of flows are convex, and the energy function is linear in both the multiplier u and the flow functions p_s, p and q, hence convex l.s.c. for fixed u and concave u.s.c. for fixed p_s, p and q. This confirms the existence of at least one saddle point, see [12, 13]. It also follows that the min and max operators of the primal-dual model (23) can be interchanged, i.e.

$$\sup_{p_s,p,q} \big\{ \inf_{u} \; E(p_s, p, q; u) \big\} \;=\; \inf_{u} \big\{ \sup_{p_s,p,q} \; E(p_s, p, q; u) \big\}\,. \qquad (25)$$

3.3 Equivalent Dual Formulation

Now we investigate the optimization of (23) by the min-max order as the righthand side of (25), i.e. we first maximize $E(p_s, p, q; u)$ over the flow functions p_s, p and q then minimize over the multiplier function u. We show that this leads to the equivalent dual model of the continuous max-flow formulation (18), i.e.

$$\min_{u} \; \big\{ D(u) \;:=\; \sum_{i=1}^{n} \big(\int_\Omega u_i(x)\, \rho(\ell_i, x)\, dx \;+\; \int_\Omega C_i(x)\, |\nabla u_i| \; dx \big) \big\} \qquad (26)$$
$$\text{s.t.} \quad \sum_{i=1}^{n} u_i(x) \;=\; 1\,, \quad u_i(x) \;\ge\; 0\,.$$

Optimization of Flow Functions p, q and p_s In order to optimize the flow function $p(x)$ in (24), let us consider the following maximization problem

$$f(q) \;=\; \sup_{p \leq C} \; p \cdot q \,. \tag{27}$$

where p, q and C are scalars.

When $q < 0$, p can be chosen to be a negative infinity value in order to maximize the value $p \cdot q$, i.e. $f(q) = +\infty$. In consequence, we must have $q \geq 0$ so as to make the function $f(q)$ meaningful. Observe now that

$$\begin{cases} \text{if } q = 0\,, \;\text{ then } p \leq C \text{ and } f(q) \text{ reaches the maximum } 0 \\ \text{if } q > 0\,, \;\text{ then } p = C \text{ and } f(q) \text{ reaches the maximum } q \cdot C \end{cases} . \tag{28}$$

By virtue of (28), we can equally express $f(q)$ by

$$f(q) \;=\; q \cdot C\,, \quad q \geq 0\,. \tag{29}$$

Applying (27) and (29) to the maximization of $E(p_s, p, q; u)$ of (24) over the sink flows $p_i(x)$, $i = 1 \ldots n$, we have

$$\sup_{p_i(x) \leq \rho(l_i, x)} \int_\Omega u_i p_i \, dx \;=\; \int_\Omega u_i(x) \rho(l_i, x) \, dx\,, \quad u_i(x) \;\geq\; 0\,,\; i = 1, \ldots, n\,. \tag{30}$$

For the maximization over the spatial flow functions $q_i(x)$, $i = 1, \ldots, n$, it is well-known [15] that

$$\sup_{|q_i(x)| \leq C_i(x)} \int_\Omega u_i \operatorname{div} q_i \, dx \;=\; \int_\Omega C_i(x) \, |\nabla u_i| \; dx\,. \tag{31}$$

Furthermore, observe the source flow function $p_s(x)$ is unconstrained, the maximization of (24) over p_s simply leads to

$$1 - \sum_{i=1}^{n} u_i(x) \;=\; 0\,, \quad \forall x \in \Omega\,. \tag{32}$$

By the results of (32), (30) and (31), it is easy to conclude that the maximization of the primal-dual model (24) over flow functions p_s, p and q boils down to its equivalent dual model (26). Therefore, we have

Proposition 2. *The continuous max-flow model* (18)*, the primal-dual model* (23) *and the dual model* (26) *are equivalent to each other, i.e.*

$$(18) \iff (23) \iff (26)\,.$$

The proof of Prop. 2 follows by the above statements.

In this work, we focus on the case when $C_i(x) = \alpha$, $\forall x \in \Omega$ and $i = 1, \ldots, n$. Obviously,

Proposition 3. *When $C_i(x) = \alpha$, $\forall x \in \Omega$ and $i = 1 \ldots n$, the dual model* (26) *amounts to the* convex relaxed Potts model (6)*. Hence, in this case,*

continuous max-flow model (18) $\iff$ *convex relaxed Potts model* (6)*.*

Its proof simply follows by Prop. 2, which is omitted here.

3.4 Variational Perspective of Flows and Cuts

Through the above analytical procedures, we can build up a variational perspective of flows and cuts, which recovers conceptions and terminologies used in graph-cuts.

Consider the maximization problem (27), for any fixed q, let some optimal p^* maximize $q \cdot p$ over $p \leq C$. By means of variations, if such $p^* < C$ strictly, its variation directly leads to $q = 0$ since the variation δp can be both negative and positive. On the other hand, for $p^* = C$, its variation under the constraint $p \leq C$ gives $\delta p < 0$, then we must have $q > 0$.

In terms of graph-cuts, some maximum flow $p^*(e) < C(e)$, over the edge $e \in \mathcal{E}$, just means the considered flow $p(e)$ does not reach its maximum or capacity $C(e)$ along the edge e, i.e. 'unsaturated'; which results the so-called 'cut' over the edge e.

In the same manner, for the maximum sink flow function $p_i^*(x)$, $i = 1 \dots n$, it is easy to see that when the flow $p_i^*(x) < \rho(l_i, x)$ at some $x \in \Omega$, i.e. 'unsaturated', we must have $u_i(x) = 0$, i.e. $u_i(x)p_i^*(x) = 0$. This means that at the position x, the flow $p_i(x)$ has no contribution to the energy function and the flow $p_i(x)$, from $x \in \Omega_i$ to the sink t, can be 'cut' off from the energy function of (23). On the other hand, in view of (10), the indicator function $u_i(x) = 0$ definitely means the position x is not labeled as l_i.

For the spatial flows $q_i^*(x)$, $i = 1 \dots n$, let

$$C_{\mathrm{TV}}^i := \{ q_i(x) \,|\, |q_i(x)| \leq C_i(x)\,,\; n \cdot q_i|_{\partial\Omega} = 0 \}\,.$$

Observe that

$$\sup_{q_i \in C_{\mathrm{TV}}^i} \int_\Omega u_i(x)\ \mathrm{div}\, q_i(x)\, dx \;=\; \sup_{p \in C_{\mathrm{TV}}^\alpha} \int_\Omega q_i(x)\, \nabla u_i(x)\, dx\,, \tag{33}$$

the extremum of the righthand in (33) just indicates the normal cone-based condition [18] of $\nabla u_i^*(x)$, i.e.

$$\nabla u_i^* \;\in\; N_{C_{\mathrm{TV}}^i}(q_i^*)\,, \tag{34}$$

for $i = 1 \dots n$.

Then we simply have:

$$\text{if} \quad \nabla u_i^*(x) \quad \neq 0\,, \qquad \text{then} \quad |q_i^*(x)| = C_i(x)\,, \tag{35a}$$

$$\text{if} \quad |q_i^*(x)| < C_i(x)\,, \qquad \text{then} \quad \nabla u_i^*(x) \quad = 0\,. \tag{35b}$$

In other words, at some locations $x \in \Omega$ where $\nabla u_i^*(x) \neq 0$, the spatial flow $q_i^*(x)$ is 'saturated' (35a), i.e. $|q_i^*(x)| = C_i(x)$; at some locations $x \in \Omega$ where $|q_i^*(x)| < \alpha$ is not saturated, we must have $\nabla u_i^*(x) = 0$, i.e. no variances of $u_i^*(x)$ around x, and therefore the 'cut' does not appear around the spatial domain at x.

4 Multiplier-Based Max-Flow Algorithm

Observe that the energy function of the primal-dual model (23) just gives the Lagrangian function of the continuous max-flow model (18) where $u_i(x)$, $i = 1 \dots n$, are

the corresponding multiplier functions to the flow conservation equalities (17). Now we introduce our multiplier-based max-flow algorithm, which is based on the augmented lagrangian method [3]. In this respect, we define the augmented Lagrangian function

$$L_c(p_s, p, q, u) \;=\; \int_\Omega p_s \, dx \;+\; \sum_{i=1}^{n} \langle u_i, \operatorname{div} q_i - p_s + p_i \rangle \;-\; \frac{c}{2} \sum_{i=1}^{n} \|\operatorname{div} q_i - p_s + p_i\|^2$$

where $c > 0$.

By the standard augmented Lagrangian method, each iteration of the algorithm can then be generalized as follows:

– Optimize spatial flows q_i, $i = 1 \dots n$, by fixing other variables:

$$q_i^{k+1} \;:=\; \arg \max_{\|q_i\|_\infty \le \alpha} \; -\frac{c}{2} \left\| \operatorname{div} q_i + p_i^k - p_s^k - u_i^k / c \right\|^2 , \tag{36}$$

which can be solved by Chambolle's projection algorithm [9].

– Optimize sink flows p_i, $i = 1 \dots n$, by fixing other variables

$$p_i^{k+1} \;:=\; \arg \max_{p_i(x) \le \rho(l_i, x)} \; -\frac{c}{2} \left\| p_i + \operatorname{div} q_i^{k+1} - p_s^k - u_i^k / c \right\|^2 , \tag{37}$$

which can be computed at each $x \in \Omega$ in a closed form.

– Optimize the source flow p_s and update multipliers u_i, $i = 1 \dots n$

$$p_s^{k+1} \;:=\; \arg \max_{p_s} \int_\Omega p_s \, dx - \frac{c}{2} \sum_{i=1}^{n} \left\| p_s - (p_i^{k+1} + \operatorname{div} q_i^{k+1}) + u_i^k / c \right\|^2 , \tag{38}$$

$$u_i^{k+1} \;= u_i^k - c \, (\operatorname{div} q_i^{k+1} - p_s^{k+1} + p_i^{k+1}) \, . \tag{39}$$

Both (38) and (39) can be obtained in the closed form.

Consider the above numerical steps, it is easy to see that the two flows q_i and p_i, $i = 1 \dots n$, computed by (36) and (37) can be handled independently for each label i. Hence, (36) and (37) can be implemented in a parallel way. Once such two steps are finished, the source flow $p_s(x)$ and the labeling functions $u_i(x)$, $i = 1 \dots n$, are updated. Obviously, such parallelism naturally originates from the configuration shown in Fig. 1.

4.1 Fast Linearized Max-Flow Based Algorithm

Actually, the sub-step (36) at each iteration can be solved in an inexact manner, i.e. without solving the Chambolle-projection exactly which is time-consuming. Now, we consider the minimizaion problem

$$q_i^{k+1}(x) \;:=\; \arg \min_{|q_i(x)| \le \alpha} \left\| \operatorname{div} q_i - D_i^k \right\|^2 \tag{40}$$

where $D_i^k(x) = (p_s^k + u_i^k / c - p_i^k)(x)$ for $i = 1 \dots n$. We propose a linearized solver which just performs a simple projection-gradient step to the proposed problem (40) such that

$$q_i^{k+1} \;:=\; q_i^k \;-\; \gamma \nabla (\operatorname{div} q_i^k - D_i^k) \tag{41}$$

where γ is the step-size and its maximum value depends on the largest eigen-value of the matrix $\nabla \operatorname{div}$ after discretization. In this work, we apply the mimetic finite-difference method [20, 19] over the regular image grid [41, 43], and the largest eigen-value of the resulting matrix $\nabla \operatorname{div}$ is just $1/8$. Hence we apply $\gamma \leq 1/4$ in the following experiments, i.e. two times of the largest eigen-value, in order to construct a nonexpansive operator for the proposed iterative updating step (42) of $q_i(x)$, $i = 1 \dots n$. Similar linearized solver appeared in the recent study of the Bregman-Splitting algorithm [16], which results in a fast solver to the continuous min-cut problem (15).

In this regard, we propose the fast linearized max-flow based algorithm as Alg. 4.1, where every substep at each iteration only performs one simple computation.

Algorithm 1 Multiplier-Based Maximal Potts Flow Algorithm

Set the starting values $p_s^1(x)$, $p^1(x)$, $q^1(x)$ and $u^1(x)$, let $k = 1$ and start k-th iteration, which includes the following steps, till convergence:

- Update q_i, $i = 1 \dots n$, by fixing other variables

$$q_i^{k+1} = q_i^k - \gamma \nabla (\operatorname{div} q_i^k - D_i^k), \tag{42}$$

  where $D_i^k(x) = (p_s^k + u_i^k/c - p_i^k)(x)$ for $i = 1 \dots n$.
- Update p_i, $i = 1 \dots n$, by solving the substep (37) which results in

$$p_i^{k+1}(x) = \min \big(\rho(l_i, x), F_i^k(x)\big)$$

  where $F_i^k(x) = (p_s^k + u_i^k/c - \operatorname{div} q_i^{k+1})(x)$ for for $i = 1 \dots n$;
- Update p_s by solving the substep (38)

$$p_s^{k+1}(x) = (1 + c \sum_{i=1}^{n} G_i^k(x))/n\, c,$$

  where $G_i^k(x) = (p_i^{k+1} + \operatorname{div} q_i^{k+1} - u_i^k)(x)/c$ for $i = 1 \dots n$.
- Update multipliers u_i, $i = 1, \dots, n$, by

$$u_i^{k+1} = u_i^k - c\,(\operatorname{div} q_i^{k+1} - p_s^{k+1} + p_i^{k+1});$$

- Let $k = k + 1$ return to the $k + 1$ iteration till converge.

5 Experiments

In this section, we first make experiments to validate the proposed continuous max-flow algorithm, i.e. Alg. 4.1, for its associated parameter settings and convergence. We then show its significant outperformance over other state of art convex optimization approaches. In comparison to graph-cuts, e.g. alpha-expansion, the studied convex relaxation model comes with the important advantage of rotational invariance, which means that metrication errors are properly avoided. The quality of the relaxation approach (6)

has been evaluated extensively in [44, 27, 2] where its outperformance over the state of art methods from discrete optimization, e.g. alpha expansion and alpha-beta swap [5] has been shown for effectively minimizing the Pott's energy. All experiments in this work are made on a Windows desktop with the intel CPU i7-920 (2.66 GHz) and the NVidia GPU Tesla C1060.

5.1 Algorithm Validations

For the proposed Alg. 4.1, there are two parameters: the step-size γ and the augmented parameter c. In view of (39), the update of the labeling function $u_i(x)$, $i = 1 \dots n$, at each iteration gives us an appropriate criterion of convergence

$$\epsilon_a \;=\; \frac{\sum_{i=1}^{n} \left| c\,(\operatorname{div} q_i^{k+1} - p_s^{k+1} + p_i^{k+1}) \right|}{n\ |\Omega|}$$

which evaluates the avarage change of the labeling function for each pixel x and each label. In the following experiments, we apply ϵ_a to be less than some small positive value as the convergence criterion.

We make labeling experiments in this part with the same input image (see Fig. 2(a) and Fig. 2(b) for the input and ground-truth images). Four data terms $\rho(l_i, x) = |I(x) - l_i|^p$, $i = 1 \dots 4$, are used, where $I(x)$ and l_i, $i = 1 \dots 4$, take the triple RGB values and $p = 1$.

In this respect, we make labeling experiments of the input image (see Fig. 2(a) and Fig. 2(b) for the input and ground-truth images) together with various step-size $\gamma = 0.1, 0.11, \dots, 0.18$ and the fixed augmented parameter $c = 0.25$. We set $\epsilon_a < 5 \times 10^{-4}$ as the stopping criterion. When $\gamma > 0.18$, the proposed algorithm fails to achieve convergence within 300 iterations and more than one updating of q_i, $i = 1 \dots n$, for each iteration are required to obtain a faster convergence. Tab. 1 list detailed results in terms of the total number of iterations and computation time. Fig. 2(d) shows their respective convergence graph with log-log illustration. Clearly, when the step-size γ takes values between 0.1 and 0.17, Alg. 4.1 performs very similarly and obtains convergence within about 35 iterations.

To evaluate Alg. 4.1 with various settings of the augmented parameter c, we make experiments for the same input along with $c = 0.1$, 0.25, 0.4, 0.55, 0.7, 0.85, 1, 2, 3 and the fixed step-size $\gamma = 0.17$. We set $\epsilon_a < 5 \times 10^{-4}$ as the stopping criterion. Tab. 2 list detailed results in terms of the total number of iterations and computation time. Fig. 2(e) shows their respective convergence graph with log-log illustration. Clearly, when the augmented parameter c takes values between 0.1 and 0.85, Alg. 4.1 converges relatively faster and obtains convergence within 40 iterations. In Fig. 2(e), the bolded black line shows the convergence result (fastest) of $c = 0.25$ and the bolded green line shows the convergence result (slowest) of $c = 3$.

5.2 Comparisons to Other Approaches

Examples are given in Figure 3, where we have used the Mumford-Shah data term $\rho(\ell_i, x) = |I(x) - \ell_i|^2$, $i = 1, ..., n$. As we see, equally good solutions as alpha expansion are produced, but without the metrication artifacts.

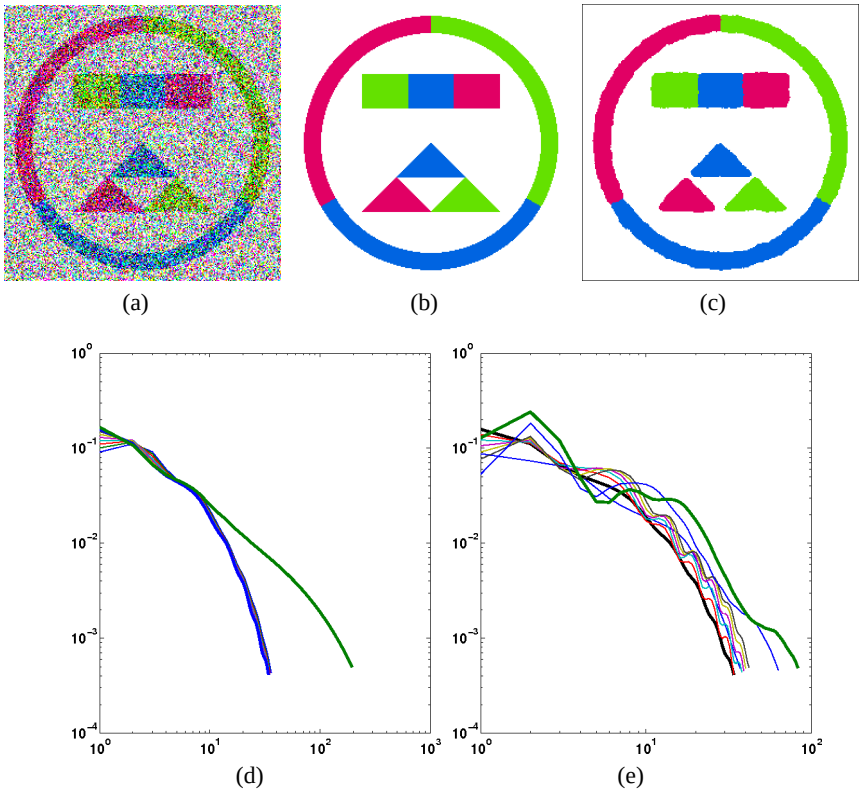

Fig. 2. (a) Input Image, (b) Ground-truth Image (c) Computation Result $u(x)$ with $\gamma = 0.17$ and $c = 0.55$, (d) Convergence results associated to different step-size settings of γ, (e) Convergence results associated to different settings of the augmented parameter c.

In contrast to the minimization approach of Zach et. al. [44], the proposed algorithm can be proved to converge by classical optimization theories. The Douglas-Rachford splitting approach given in [27] can also be proved to converge, but we experienced that our approach was more efficient than both these approaches. The inner problem has the same complexity for all approaches, since it is dominated by the process of iteratively solve a tv minimization problem. However, in contrast to [44, 27] our approach avoids iterative projections to the convex set S and consequently require much less outer iterations. Convergence is reached for a wide range of the outer 'step-size' c. To measure converge, we find a good estimate of the final energy E^* by solving the problem with 10000 outer iterations. The energy precision at iteration k is then measured by $\epsilon = \frac{E^k - E^*}{E^*}$. For the three images (see Fig. 2), different precision ϵ are taken and the total number of iterations to reach convergence is evaluated, see Tab 3: clearly, our method is about 4 times faster than the Douglas-Rachford-splitting [27], the approach in [44] is even slower and failed to reach such a low precision.

Table 1. Validation for the step-size γ when $c = 0.25$

γ	0.10	0.11	0.12	0.13	0.14	0.15	0.16	0.17	0.18
Iter.	36	35	35	34	34	34	34	34	195
Time (sec.)	0.91	0.85	0.84	0.82	0.80	0.82	0.82	0.81	4.63

Table 2. Validation for the augmented parameter c when $\beta = 0.18$

c	0.1	0.25	0.4	0.55	0.7	0.85	1	2	3
Iter.	37	34	34	38	39	40	42	63	83
Time (sec.)	0.93	0.82	0.82	0.92	0.94	0.97	1.01	1.52	2.02

6 Conclusions

In this paper, we introduced and investigated a novel continuous max-flow model which is dual to a convex relaxation of Potts problem, and resulted in a new variational perspective of flows and cuts in the spatially continuous configuration and properly recovered close connections between flows and cuts. Moreover, in comparison to previous efforts which are trying to compute the optimal labeling functions in a direct way, we proposed a new multiplier-based max-flow algorithm. The main advantages of such max-flow based algorithm are: it avoids extra computation load to explicitly explore the pointwise simplex constraint, each flow function is updated in a simple way; in addition, its numerical scheme contains a natural parallel framework, which can be easily accelerated by the modern parallel computation hardware, e.g. GPU. Numerical experiments showed it outperformed state of art approaches in terms of quality and efficiency.

Acknowledgements: This research has been supported by Natural Sciences and Engineering Research Council of Canada (NSERC) Accelerator Grant R3584A04, the Norwegian Research Council (eVita project 166075), MOE (Ministry of Education) Tier II project T207N2202 and IDM project NRF2007IDMIDM002-010.

	Brain $\epsilon \leq 10^{-5}$	Flower $\epsilon \leq 10^{-4}$	Bear $\epsilon \leq 10^{-4}$
Zach et al [44]	fail to reach such a precision		
Lellmann et al [27]	421 iter.	580 iter.	535 iter.
Proposed algorithm	88 **iter.**	147 **iter.**	133 **iter.**

Table 3. Comparisons between algorithms: Zach et al [44], Lellmann [27] and the proposed max-flow algorithm: for the three images (see Fig. 2), different precision ϵ are taken and the total number of iterations to reach convergence is evaluated.

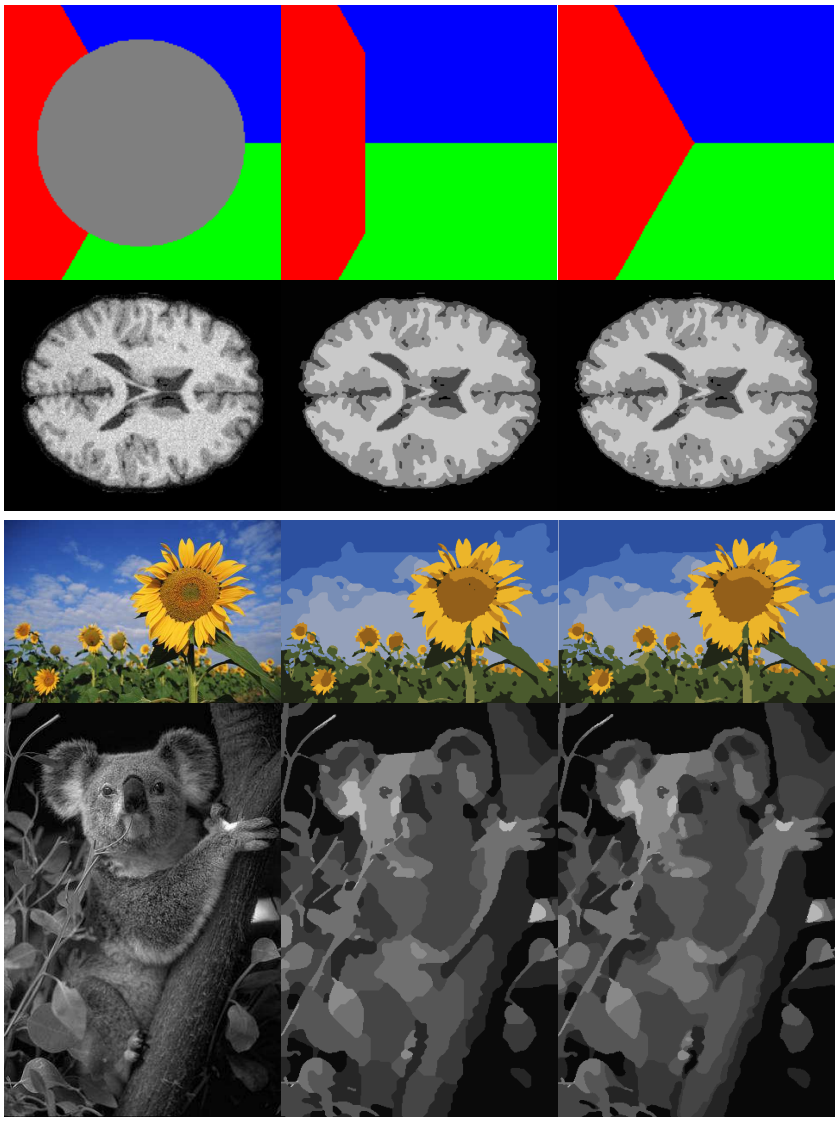

Fig. 3. Each row (from left to right): the input image, result by Alpha expansion with 8 neighbors, result by the proposed max-flow approach. For the experiment in 1st row (inpainting in gray area), $\alpha = 0.03$ and $n = 3$; 2nd row, $\alpha = 0.04$ and $n = 4$, 3rd row, $\alpha = 0.047$ and $n = 10$; 4th row, $\alpha = 0.02$ and $n = 8$.

References

1. E. Bae, J. Yuan, X.-C. Tai, and Y. Boycov. A fast continuous max-flow approach to non-convex multilabeling problems. Technical report CAM-10-62, UCLA, submitted to a journal,

2010.
2. Egil Bae, Jing Yuan, and Xue-Cheng Tai. Global minimization for continuous multiphase partitioning problems using a dual approach. *International Journal of Computer Vision*, 92(1):112–129, 2011.
3. Dimitri P. Bertsekas. *Nonlinear Programming*. Athena Scientific, September 1999.
4. Y. Boykov and V. Kolmogorov. Computing geodesics and minimal surfaces via graph cuts. In *ICCV 2003*, pages 26–33, 2003.
5. Yuri Boykov, Olga Veksler, and Ramin Zabih. Fast approximate energy minimization via graph cuts. *IEEE Transactions on PAMI*, 23:1222 – 1239, 2001.
6. X. Bresson, S. Esedoglu, P. Vandergheynst, J.P. Thiran, and S. Osher. Fast global minimization of the active contour/snake model. *Journal of Mathematical Imaging and Vision*, 28(2):151–167, 2007.
7. Thomas Brox and Joachim Weickert. Level set segmentation with multiple regions. *IEEE Transactions on Image Processing*, 15(10):3213–3218, 2006.
8. A. Chambolle, D. Cremers, and T. Pock. A convex approach for computing minimal partitions. Technical Report TR-2008-05, University of Bonn, November 2008.
9. Antonin Chambolle. An algorithm for total variation minimization and applications. *Journal of Mathematical Imaging and Vision*, 20(1):89–97, January 2004.
10. T. Chan and L.A. Vese. *Active contours without edges*. IEEE Image Proc., 10, pp. 266-277, 2001.
11. Thomas H Cormen, Charles E Leiserson, Ronald L Rivest, and Clifford Stein. *Introduction to Algorithms*. MIT Press, Cambridge, MA, second edition, 2001.
12. Ivar Ekeland and Roger Téman. *Convex analysis and variational problems*. Society for Industrial and Applied Mathematics, Philadelphia, PA, USA, 1999.
13. Ky Fan. Minimax theorems. *Proc. Nat. Acad. Sci. U. S. A.*, 39:42–47, 1953.
14. L. R. Ford and D. R. Fulkerson. *Flows in Networks*. Princeton University Press, 1962.
15. Enrico Giusti. *Minimal surfaces and functions of bounded variation*. Australian National University, Canberra, 1977.
16. Tom Goldstein, Xavier Bresson, and Stanley Osher. Geometric applications of the split bregman method: Segmentation and surface reconstruction. Technical report CAM09-06, UCLA, CAM, 2009.
17. D. M. Greig, B. T. Porteous, and A. H. Seheult. Exact maximum a posteriori estimation for binary images. *J. Royal Stat. Soc., Series B*, pages 271–279, 1989.
18. Jean-Baptiste Hiriart-Urruty and Claude Lemaréchal. *Convex analysis and minimization algorithms. I*. Springer-Verlag, Berlin, 1993. Fundamentals.
19. J. M. Hyman and M. J. Shashkov. Adjoint operators for the natural discretizations of the divergence, gradient and curl on logically rectangular grids. *Appl. Numer. Math.*, 25(4):413–442, 1997.
20. J. M. Hyman and M. J. Shashkov. Natural discretizations for the divergence, gradient, and curl on logically rectangular grids. *Comput. Math. Appl.*, 33(4):81–104, 1997.
21. Hiroshi Ishikawa. Exact optimization for markov random fields with convex priors. *IEEE Transactions on PAMI*, 25:1333–1336, 2003.
22. Pushmeet Kohli, M. Pawan Kumar, and Philip H.S. Torr. p^3 and beyond: Move making algorithms for solving higher order functions. *IEEE Transactions on PAMI*, 31(9):1645–1656, 2009.
23. Vladimir Kolmogorov and Yuri Boykov. What metrics can be approximated by geo-cuts, or global optimization of length/area and flux. In *In ICCV*, pages 564–571, 2005.
24. Vladimir Kolmogorov and Ramin Zabih. What energy functions can be minimized via graph cuts. *IEEE Transactions on PAMI*, 26:65–81, 2004.
25. Nikos Komodakis and Georgios Tziritas. Approximate labeling via graph-cuts based on linear programming. In *Pattern Analysis and Machine Intelligence*, pages 1436–1453, 2007.

26. J. Lellmann, F. Becker, and C. Schnörr. Convex optimization for multi-class image labeling with a novel family of total variation based regularizers. In *IEEE International Conference on Computer Vision (ICCV)*, pages 646 – 653, 2009.
27. Jan Lellmann, Jörg Kappes, Jing Yuan, Florian Becker, and Christoph Schnörr. Convex multi-class image labeling by simplex-constrained total variation. In *SSVM '09*, pages 150–162, 2009.
28. Jan Lellmann, Frank Lenzen, and Christoph Schnörr. Optimality bounds for a variational relaxation of the image partitioning problem. In *EMMCVPR*, pages 132–146, 2011.
29. Stan Z. Li. *Markov random field modeling in image analysis*. Springer-Verlag New York, Inc., Secaucus, NJ, USA, 2001.
30. J. Lie, M. Lysaker, and X.-C. Tai. A variant of the level set method and applications to image segmentation. *Math. Comp.*, 75(255):1155–1174, 2006.
31. J. Lie, M. Lysaker, and X.C. Tai. A binary level set model and some applications to Mumford-Shah image segmentation. *IEEE Img. Proc.*, 15(5):1171–1181, 2006.
32. Mila Nikolova, Selim Esedoglu, and Tony F. Chan. Algorithms for finding global minimizers of image segmentation and denoising models. *SIAM J. App. Math.*, 66(5):1632–1648, 2006.
33. S. Osher and J.A. Sethian. Fronts propagating with curvature dependent speed: algorithms based on hamilton-jacobi formulations. *J. Comput. Phys.*, 79(1):12–49, 1988.
34. Nikos Paragios, Yunmei Chen, and Olivier Faugeras. *Handbook of Mathematical Models in Computer Vision*. Springer-Verlag New York, Inc., Secaucus, NJ, USA, 2005.
35. T. Pock, A. Chambolle, H. Bischof, and D. Cremers. A convex relaxation approach for computing minimal partitions. In *CVPR*, Miami, Florida, 2009.
36. Thomas Pock, Thomas Schoenemann, Gottfried Graber, Horst Bischof, and Daniel Cremers. A convex formulation of continuous multi-label problems. In *ECCV 2008*, 2008.
37. Renfrey B. Potts. Some generalized order-disorder transformations. *In Proceedings of the Cambridge Philosophical Society, Vol. 48*, pages 106–109, 1952.
38. Martin Wainwright, Tommi Jaakkola, and Alan Willsky. Map estimation via agreement on (hyper)trees: Message-passing and linear programming approaches. *IEEE Transactions on Information Theory*, 51:3697–3717, 2002.
39. J. Yuan, E. Bae, X.-C. Tai, and Y. Boycov. A study on continuous max-flow and min-cut approaches. Technical report CAM-10-61, UCLA, 2010.
40. J. Yuan, E. Bae, and X.C. Tai. A study on continuous max-flow and min-cut approaches. In *CVPR*, USA, San Francisco, 2010.
41. J. Yuan, C. Schnörr, and G. Steidl. Simultaneous optical flow estimation and decomposition. *SIAM J. Scientific Computing*, 29(6):2283–2304, 2007.
42. Jing Yuan, Egil Bae, Xue-Cheng Tai, and Yuri Boykov. A continuous max-flow approach to potts model. In *ECCV*, 2010.
43. Jing Yuan, Christoph Schnörr, and Etienne Memin. Discrete orthogonal decomposition and variational fluid flow estimation. *Journ. of Mathematical Imaging and Vison*, pages 267–278, 2006.
44. C. Zach, D. Gallup, J.-M. Frahm, and M. Niethammer. Fast global labeling for real-time stereo using multiple plane sweeps. In *VMV 2008*, 2008.